Supporting Information

Ding and Dokholyan 10.1073/pnas.0803266105

SI Text

DMD. A detailed description of the DMD algorithm can be found elsewhere (1–3). Briefly, interatomic interactions in DMD are governed by square-well potential functions. Neighboring interactions (such as bonds, bond angles, and dihedrals) are modeled by infinitely deep square well potentials. During a simulation, an atom's velocity remains constant until a potential step is encountered, upon which time it changes instantaneously according to the conservations of energy, momentum, and angular momentum. Simulations proceed as a series of such collisions, with a rapid sorting algorithm used at each step to determine the following collision.

The difference between DMD and traditional molecular dynamics is in the interaction potential functions. Approximating continuous potentials with step functions of pairwise distances, DMD simulations are reduced to event-driven (collision) molecular dynamics. The sampling efficiency of DMD over traditional molecular dynamics is caused mainly by rapid processing of collision events and localized updates of collisions (only collided atoms are required to update at each collision). At an adequately small step size, the discrete step function approaches the continuous potential function and DMD simulations become equivalent to traditional molecular dynamics.

Metal Binding and Disulfide Bond. We modeled the metal binding by assigning distance constraints between metal atom and the corresponding metal-coordinating atoms: namely between the copper ion and ND1 of His-46, NE2 of His-48, NE2 of His-63, and NE3 of His-120; and between the zinc ion and ND1 of His-63, ND1 of His-71, ND1 of His-80, and OD1 of Asp-83. We used a square-well potential with infinitely high boundary to model the distance constraints. We used the distance in the crystal structure (Protein Data Bank ID code 2v0a) as the average distance, $\langle d \rangle$ and of the constraint and allowed 2% deviation from the average $[0.98\langle d \rangle, 1.02\langle d \rangle]$.

We used the reaction algorithm to model the distance and angular dependence of disulfide bond formation (4). For a disulfide bond formation between Cys i and Cys j, we introduced the auxiliary interactions between $S_{\gamma i}$ and $C_{\beta j}$ and between $C_{\beta i}$ and $S_{\gamma j}$ beside the interaction between $S_{\gamma i}$ and $S_{\gamma j}$ (Fig. S2). The interaction potentials were assigned in such a way the lowest energy configuration of $C_{\beta i}$-$S_{\gamma i}$–$S_{\gamma j}$-$C_{\beta j}$ corresponds to the conventional configuration observed in the Protein Data Bank (Fig. S2). For the oxidative condition, we assigned a total energy of 12 kcal/mol for a disulfide bond. For the reduced condition, we used a total energy of 1.2 kcal/mol.

Replica Exchange DMD. Efficient exploration of the potential energy landscape of molecular systems is the central theme of most molecular modeling applications. The ruggedness and the slope toward the energy minimum in the landscape govern sampling efficiency at a given temperature. Although escape out of local minima is accelerated at higher temperatures, the free energy landscape is altered due to larger entropic contributions. To efficiently overcome energy barriers while maintaining conformational sampling corresponding to a relevant free energy surface, we used the replica exchange sampling scheme (5, 6). In replica exchange computing, multiple simulations or replicas of the same system are performed in parallel at different temperatures. Individual simulations are coupled through Monte Carlo-based exchanges of simulation temperatures between replicas at periodic time intervals. Temperatures are exchanged between two replicas, i and j, maintained at temperatures T_i and T_j and with energies E_i and E_j according to the canonical Metropolis criterion with the exchange probability p, where $p = 1$ if $\Delta = (1/k_B T_i - 1/k_B T_j)(E_j - E_i) \leq 0$, and $p = \exp(-\Delta)$, if $\Delta > 0$. In DMD simulations, we used an Anderson thermostat to maintain constant temperature in simulations (7).

WHAM. We used the MMTSB tool (8) to perform WHAM analysis using replica-exchange trajectories. In short, the WHAM method uses multiple simulation trajectories with overlapping sampling along the reaction coordinates. The density of states $\rho(E)$ is self-consistently computed by combining histograms from different simulation trajectories (9). Given the density of states, the folding specific heat (C_v) can be computed at different temperatures according to the partition function, $Z = \int \rho(E) \exp(-E/K_B T) dE$. To compute the PMF as the function of reaction coordinate A, we computed the conditional probability $P(A|E)$ of observing A at given energy E, which was evaluated from all of the simulation trajectories. The PMF was computed as $PMF(A) = -\ln(\int P(A|E)\rho(E)\exp(-E/K_B T)dE) + C$. Here, the reference constant, C, was set in such a way that the lowest PMF always corresponded to zero. Because our simulations started from fully extended conformations, we excluded the trajectories from the first 5×10^5 time units and used those of the last 1.5×10^6 time units for WHAM analysis. We used the trajectories from all replicas to compute the histograms.

1. Dokholyan NV, Buldyrev SV, Stanley HE, Shakhnovich EI (1998) Discrete molecular dynamics studies of the folding of a protein-like model. *Fold Des* 3:577–587.
2. Rapaport DC (1997) *The Art of Molecular Dynamics Simulations* (Cambridge Univ Press, Cambridge, UK).
3. Zhou Y, Karplus M (1997) Folding thermodynamics of a model three-helix-bundle protein. *Proc Natl Acad Sci USA* 94:14429–14432.
4. Ding F, Borreguero JM, Buldyrey SV, Stanley HE, Dokholyan NV (2003) Mechanism for the α-helix to β-hairpin transition. *Proteins* 53:220–228.
5. Zhou R, Berne BJ, Germain R (2001) The free energy landscape for β hairpin folding in explicit water. *Proc Natl Acad Sci USA* 98:14931–14936.
6. Okamoto Y (2004) Generalized-ensemble algorithms: Enhanced sampling techniques for Monte Carlo and molecular dynamics simulations. *J Mol Graphics Model* 22:425–439.
7. Andersen HC (1980) Molecular dynamics simulations at constant pressure and/or temperature. *J Chem Phys* 72:2384–2393.
8. Feig M, Karanicolas J, Brooks CL, III (2004) MMTSB Tool Set: Enhanced sampling and multiscale modeling methods for applications in structural biology. *J Mol Graphics Model* 22:377–395.
9. Kumar S, Bouzida D, Swendsen RH, Kollman PA, Rosenberg JM (1992) The weighted histogram analysis method for free-energy calculations on biomolecules. 1. The method. *J Comput Chem* 13:1011–1021.

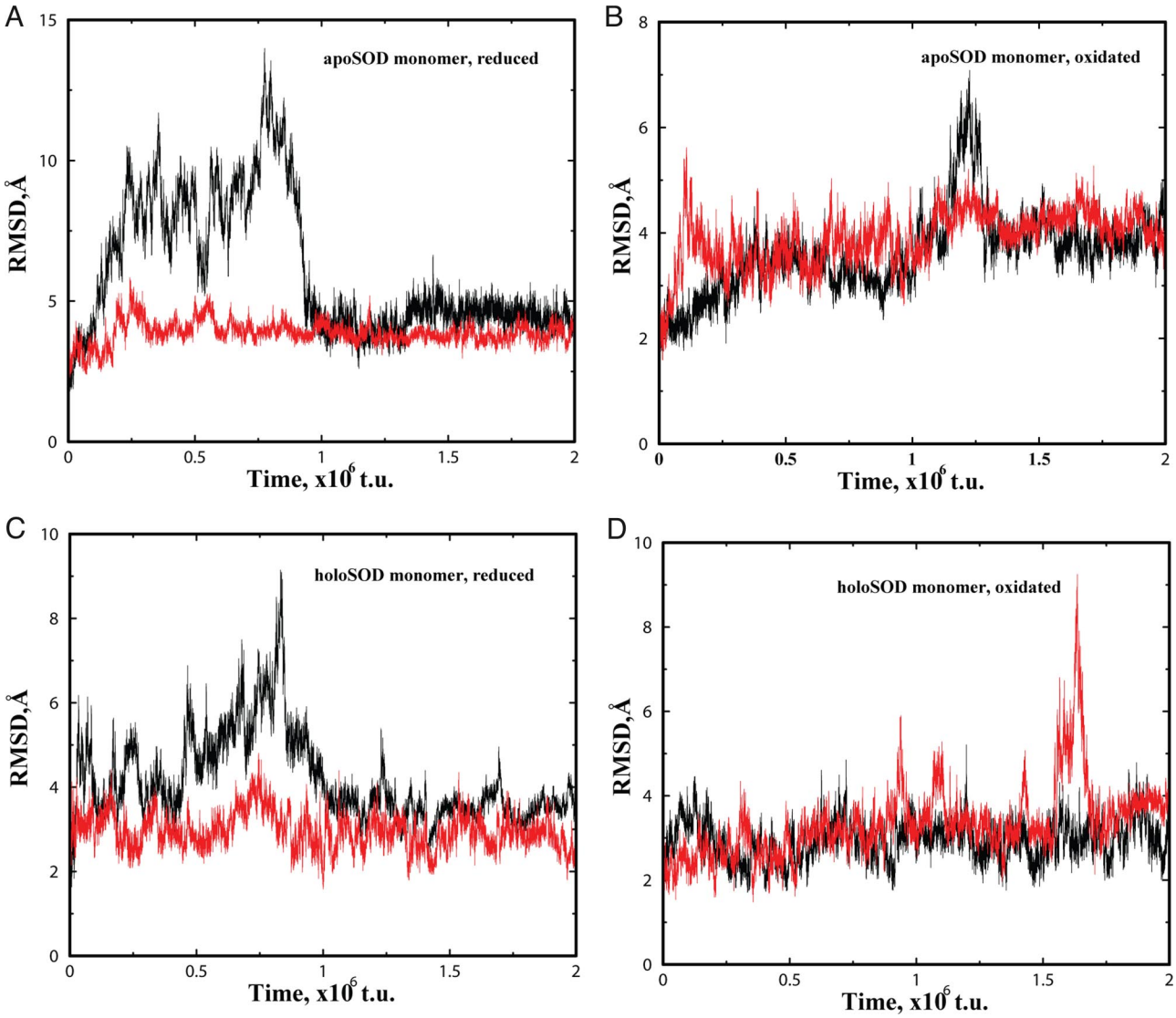

Fig. S1. The partial refolding of SOD1 monomers in DMD simulations. (*A*) ApoSOD1 monomer without disulfide bond. (*B*) ApoSOD1 monomer with disulfide bond. (*C*) HoloSOD1 monomer without disulfide bond. (*D*) HoloSOD1 monomer with disulfide bond. For each type of SOD1 monomers, there were 12 replicas running DMD simulations in parallel. For illustration purposes, we only show trajectories of two replicas where the protein stays folded or experiences partial unfolding.

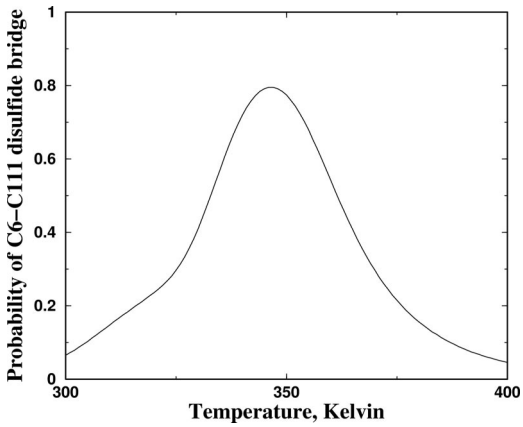

Fig. S2. The average probability to form the nonnative Cys-6–Cys-111 disulfide bridge in simulations of apoSOD1 monomer under oxidative condition. The nonnative disulfide bond has a higher probability to form after the unfolding transition (≈325 K, the highest peak in the specific heat plot in Fig. 1*B*) and has the highest probability to form near $T \approx 350$ K, corresponding to the second peak in the specific heat. At high temperatures $T > 350$ K, the disulfide bond is weakened by thermofluctuations.

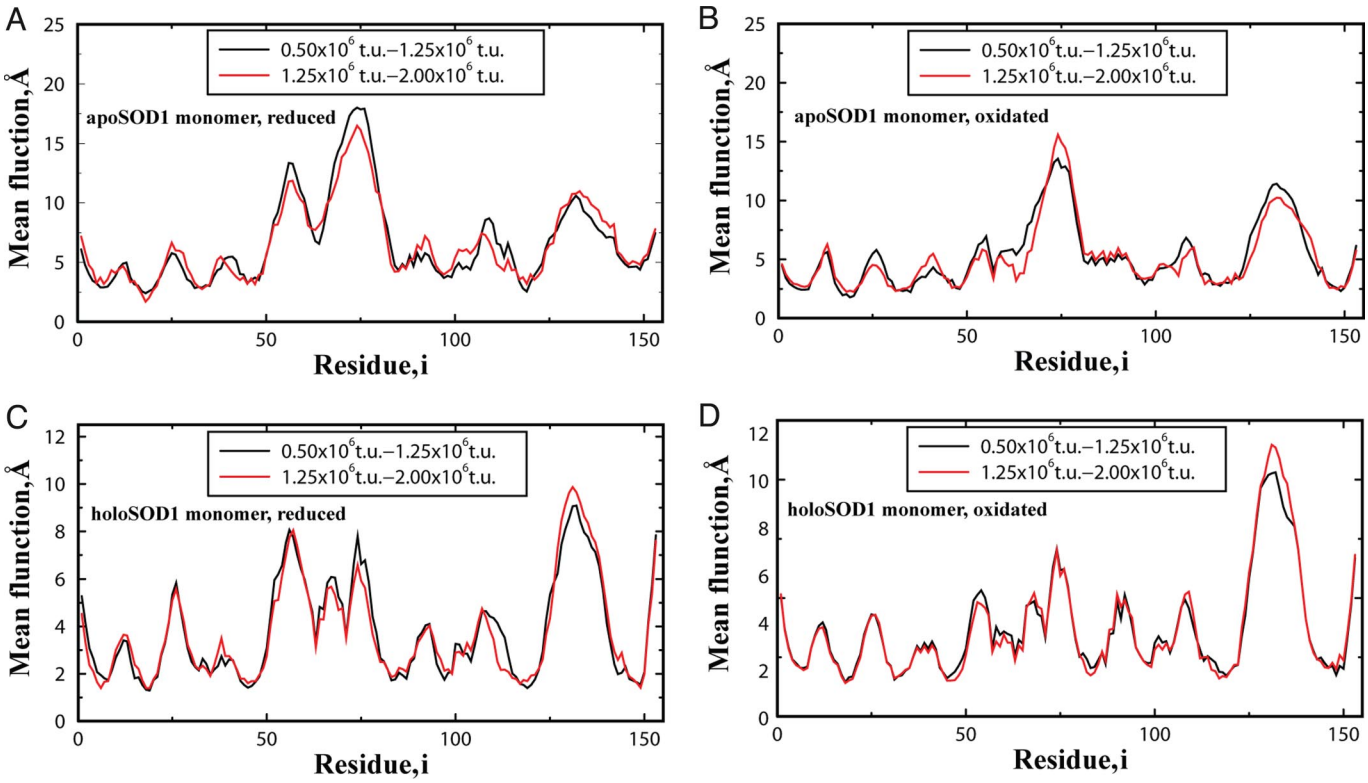

Fig. S3. The RMSF of each residue around its average structure of the folded state ensemble of SOD1. (*A*) ApoSOD1 monomer without disulfide bond. (*B*) ApoSOD1 monomer with disulfide bond. (*C*) HoloSOD1 monomer without disulfide bond. (*D*) HoloSOD1 monomer with disulfide bond. To reduce the artifact of conformational relaxation from the starting X-ray crystallography structure, we used the last three-quarters of the simulation trajectories (0.5 × 106 to 2.0 × 106 time units) to analyze the conformational dynamics. To test whether the DMD simulations sufficiently sample the conformational space of folded SOD1, we divided the last three-quarters of simulations into halves (0.5 × 106 to 1.25 × 106 time units, and 1.25 × 106 to 2.0 × 106 time units) and compute the RMSFs for each of the half trajectories separately. We found that the conformational fluctuations are consistent with each other, suggesting the sufficient sampling of the folded state of SOD1 and the robustness of the simulation results.

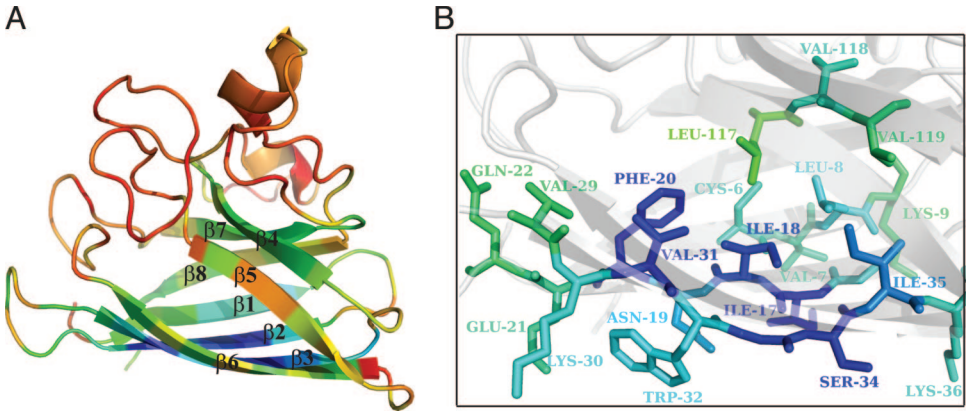

Fig. S4. The propensity of local unfolding in disulfide-reduced apoSOD1 monomer. (*A*) The cartoon representation of SOD1 monomer is colored according to the average *Q* value of disulfide-reduced apoSOD1 monomer. The residues with low average *Q* values are in red, and those with high *Q* values are in blue. (*B*) The residues with average *Q* >60% are shown in stick form.

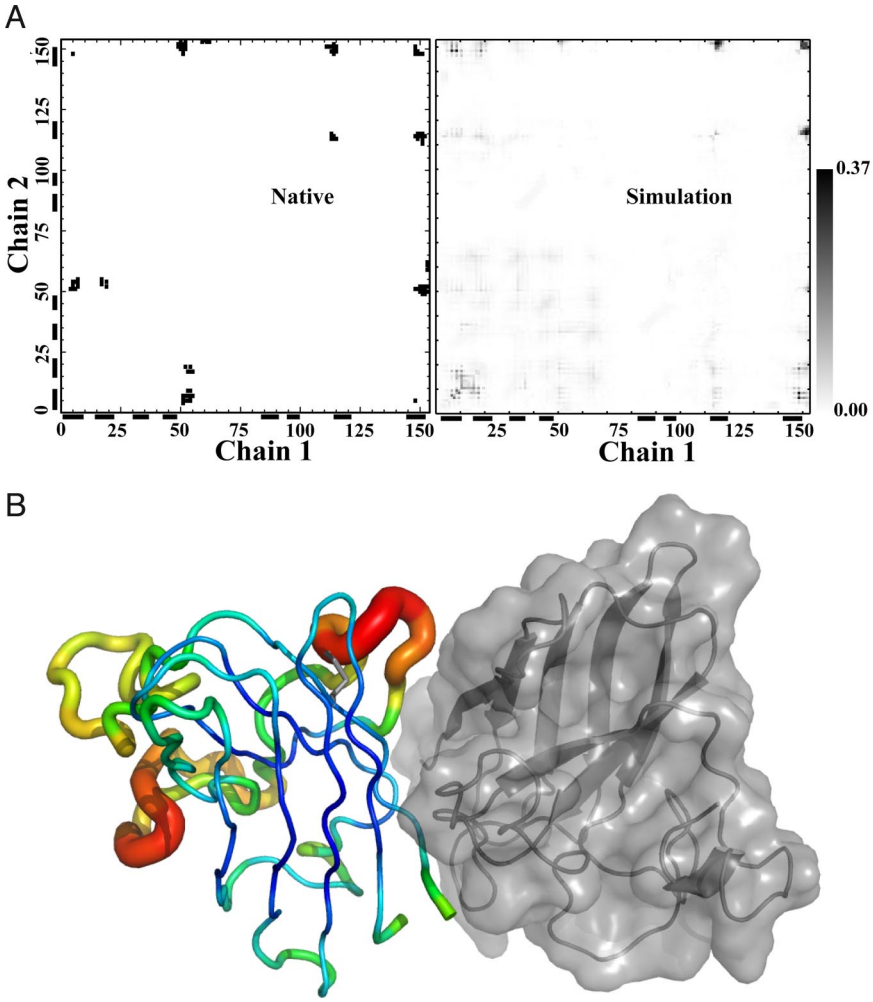

Fig. S5. The interdomain contact frequency of disulfide-reduced apoSOD1 dimer. (*A*) (*Right*) The interdomain contact frequency map is colored in grayscale. (*Left*) For comparison, the native interdomain contact map is shown. (*B*) In the SOD dimer, one monomer is in tube representation with color and backbone radius assigned according to the corresponding rmsd and the other is shown with its molecular surface in gray.

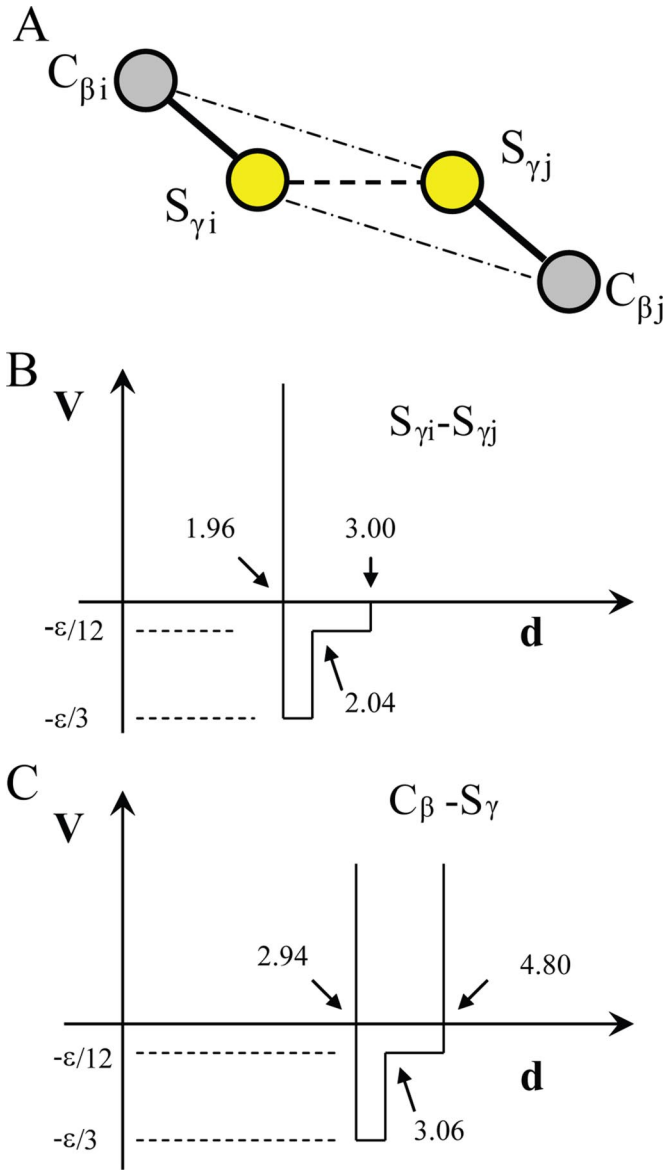

Fig. S6. The schematic diagram for disulfide bond formation. (*A*) We added auxiliary interactions between $C_{\beta i}$ and $S_{\gamma j}$ and between $C_{\beta j}$ and $S_{\gamma i}$ to impose the angular dependence of the disulfide bond. For a disulfide bond, the average distance between $S_{\gamma i}$ and $S_{\gamma j}$ was 2.0 Å, and the average distance between $C_{\beta i}$ and $S_{\gamma j}$ (between $C_{\beta j}$ and $S_{\gamma i}$) was 3.0 Å. (*B*) We used an interaction range of 3.0 Å between $S_{\gamma i}$ and $S_{\gamma j}$. The energy ε corresponds to the total energy of a disulfide bond. When two atoms $S_{\gamma i}$ and $S_{\gamma j}$ came to the interaction range of disulfide bond interaction, we evaluated the total potential energy change by checking the two auxiliary bonds. (*C*) The potential energy of the auxiliary bond is shown. If the kinetic energy is enough to overcome the potential energy change (in the case of unfavorable orientation), the two Cys forms hydrogen-bond successfully.